Coupling of laser energy into plasma channels

D. A. Dimitrov, R. E. Giacone, D. L. Bruhwiler, and R. Busby
Tech-X Corporation, 5621 Arapahoe Avenue, Suite A, Boulder, Colorado 80303

J. R. Cary
Tech-X Corporation, 5621 Arapahoe Avenue, Suite A, Boulder, Colorado 80303
and University of Colorado, Boulder, Colorado 80309

C. G. R. Geddes, E. Esarey, and W. P. Leemans
Lawrence Berkeley National Laboratory, 1 Cyclotron Road, Berkeley, California 94720

(Received 28 July 2006; accepted 9 March 2007; published online 30 April 2007)

Diffractive spreading of a laser pulse imposes severe limitations on the acceleration length and maximum electron energy in the laser wake field accelerator (LWFA). Optical guiding of a laser pulse via plasma channels can extend the laser-plasma interaction distance over many Rayleigh lengths. Energy efficient coupling of laser pulses into and through plasma channels is very important for optimal LWFA performance. Results from simulation parameter studies on channel guiding using the particle-in-cell (PIC) code VORPAL [C. Nieter and J. R. Cary, J. Comput. Phys. **196**, 448 (2004)] are presented and discussed. The effects that density ramp length and the position of the laser pulse focus have on coupling into channels are considered. Moreover, the effect of laser energy leakage out of the channel domain and the effects of tunneling ionization of a neutral gas on the guided laser pulse are also investigated. Power spectral diagnostics were developed and used to separate pump depletion from energy leakage. The results of these simulations show that increasing the density ramp length decreases the efficiency of coupling a laser pulse to a channel and increases the energy loss when the pulse is vacuum focused at the channel entrance. Then, large spot size oscillations result in increased energy leakage. To further analyze the coupling, a differential equation is derived for the laser spot size evolution in the plasma density ramp and channel profiles are simulated. From the numerical solution of this equation, the optimal spot size and location for coupling into a plasma channel with a density ramp are determined. This result is confirmed by the PIC simulations. They show that specifying a vacuum focus location of the pulse in front of the top of the density ramp leads to an actual focus at the top of the ramp due to plasma focusing, resulting in reduced spot size oscillations. In this case, the leakage is significantly reduced and is negligibly affected by ramp length, allowing for efficient use of channels with long ramps. © *2007 American Institute of Physics*. [DOI: 10.1063/1.2721068]

I. INTRODUCTION

A short (~50 fs), intense (~10^{18} W/cm^2) laser pulse in a laser wakefield accelerator (LWFA) can excite and sustain very high longitudinal electric fields (greater than 100 GV/m) that may allow acceleration of particles to very high energies (greater than 100 MeV) in extremely short distances (few millimeters).[1] More precisely, ionized plasmas can sustain electron plasma waves (EPW) with longitudinal electric fields on the order of the nonrelativistic wave-breaking field, $E_0=cm_e\omega_p/e$. For a typical electron density of $n_e=10^{18}$ cm^2, the electric field is $E_0\approx 100$ GV/m, which is approximately three orders of magnitude greater than the maximum obtained in conventional rf linacs. A correctly placed trailing electron bunch can be accelerated by the longitudinal electric field and focused by the transverse electric field of the plasma wake.

Demonstration of a 1 GeV LWFA module, a common goal for the plasma-based accelerator community, has recently been achieved.[2] In order to reach 1 GeV energies, the laser must be kept focused over many Rayleigh lengths. In the absence of optical guiding, the spreading of the laser beam due to diffraction imposes a severe limitation to the acceleration length and, therefore, the maximum energy to which a charged particle can be accelerated. The interaction length is effectively limited to less than one Rayleigh length.

Optical guiding of a laser pulse in the LWFA via plasma channels can greatly increase the interaction length and, hence, the maximum energy of trapped electrons.[3–5] Energy efficient coupling of laser pulses from vacuum into plasma channels is very important for optimal LWFA performance. In this paper, we have studied these issues by performing two-dimensional (2D) particle-in-cell (PIC) simulations using the VORPAL[6] code.

We define the *vacuum focus* to be the waist location of the laser pulse in the absence of plasma. In the presence of a preionized plasma channel, with a density ramp that is assumed to include partial channel formation (see Sec. III and Fig. 3 for details), the converging laser pulse is partially focused by the density ramp. Hence, if the vacuum focus is placed at the top of the density ramp (i.e., the channel entrance) with the matched spot size, one finds that the pulse is overfocused (the spot size is too small for the channel) and

this mismatch leads to subsequent spot size oscillations, often referred to as betatron oscillations.

We study the coupling of the laser pulse with the channel by varying the length of the plasma ramp and position of the laser focus inside the density ramp. Oscillations of the laser spot size inside the channel are tracked to determine an optimum matching between the pulse and channel. Using power spectral diagnostics, we determined how pump depletion and leakage are affected by inefficient coupling. The power spectral diagnostics show that pump depletion and leakage increase with the amplitude of the spot size oscillations.

Moreover, we used the source-dependent expansion (SDE)[1,7,8] to derive an ordinary differential equation that describes the evolution of the laser spot size in the ramp density profiles we simulated. We obtain the optimal vacuum focus location and spot size to optimally match a laser pulse for given ramp density profile parameters from a numerical solution of this equation. The result is of considerable importance. It indicates that the vacuum focus has to be placed in the ramp and not at its end when the channel starts. Furthermore, the vacuum focus spot size has to be larger than the channel radius. The deviations of the vacuum focus location from the location of the channel entrance and the vacuum spot size from the channel radius increase with the length of the ramp. The PIC simulations confirm the prediction of the theory and show that after appropriate modification of the vacuum laser focus location and spot size, the betatron oscillations are effectively suppressed. In turn, this significantly reduces the leakage of laser energy transversely (outside of the domain of the channel). This allows coupling with negligible reduction in efficiency for ramps up to two Rayleigh lengths.

For the laser and plasma parameters considered here, roughly 10–15% of the laser pulse energy is seen to leak transversely through the channel walls, roughly an order of magnitude more energy than is lost via pump depletion. The goal of an LWFA is to convert laser energy as efficiently as possible into a strong plasma wake, so as to maximize the charge and energy of the accelerated electron distribution. Careful matching of the laser pulse into the channel can reduce the energy leakage by roughly a factor of 2, independent of the density channel length (see Tables I and II for details). The work presented here provides a physical explanation for how minor adjustments of the expected spot size and location in the laboratory can result in order-of-magnitude changes to the total pulse energy emerging from the plasma channel. In particular, this work indicates that it would be fruitful to investigate other ways of making the walls of a plasma density channel more ideal and less leaky.

The remainder of this paper is organized as follows. In Sec. II, simulations to study energy coupling of a laser pulse into a plasma channel are presented. Effects that tunneling ionization has on energy loss when coupling to and propagating inside channels are shown in Sec. III. We summarize the results of this study in Sec. IV. In the Appendix, we describe diagnostic tools developed to track energy loss caused by pump depletion and leakage.

TABLE I. The pump depletion and leakage are calculated from the power spectral diagnostic for varying ramp lengths when the laser pulse is vacuum focused at the entrance of the plasma channel and the vacuum waist is held constant at 6 μm. The values in parentheses for the pulse location indicate the distance it has traveled in the channel (the channel entrance is at the top of the ramp). The values for the pump depletion and leakage are rounded to the first digit after the decimal point.

Ramp length	Pulse location	P_{pd} (%)	$P_{lk}^{[-r_0,r_0]}$ (%)	$P_{lk}^{[-2r_0,2r_0]}$ (%)
$1Z_R$ (141 μm)	188 μm ($0.1Z_R$)	0.0	1.9	0.0
	636 μm ($3.3Z_R$)	0.4	3.5	1.7
	1344 μm ($8.3Z_R$)	0.9	9.1	2.8
$1.5Z_R$ (212 μm)	270 μm ($0.2Z_R$)	0.2	0.4	0.1
	1173 μm ($6.6Z_R$)	0.8	8.8	5.3
	1515 μm ($9Z_R$)	1.1	5.1	4.1
$2Z_R$ (282 μm)	311 μm ($0.0Z_R$)	0.2	0.8	0.7
	1312 μm ($7.1Z_R$)	1.4	12.2	6.6
	1597 μm ($9.1Z_R$)	1.3	13.8	9.1

II. COUPLING OF LASER PULSES INTO A PLASMA CHANNEL

In this section, we consider coupling of laser pulses into preionized plasma channels. In experiments, the entrance of a plasma channel is preceded by a density ramp that can be as long as a few Rayleigh lengths. For an optimal guiding of a laser pulse in a plasma channel, the location of the pulse waist has to be matched to the entrance of the channel. In vacuum, the spot size of a laser pulse as a function of the propagation distance is known.[9,10] In this case, it is straightforward to launch a laser pulse in a simulation (or an experiment) and know *a priori* where the location x_f of the pulse waist will be. For the simulation results presented here, we launched laser pulses that are linearly polarized along the ignorable direction z and are loaded in the simulations using the functional form[9,10] (in vacuum)

TABLE II. The pump depletion and leakage are calculated from the power spectral diagnostic for different ramp lengths when the optimal laser pulse vacuum focus is determined from Eq. (8) and its waist from Eq. (7). The values in parentheses for the pulse location indicate the distance it has traveled in the channel (after the top of the ramp).

Ramp length	Pulse location	P_{pd} (%)	$P_{lk}^{[-r_0,r_0]}$ (%)	$P_{lk}^{[-2r_0,2r_0]}$ (%)
$1Z_R$ (141 μm)	188 μm ($0.1Z_R$)	0.0	4.4	0.0
	636 μm ($3.3Z_R$)	0.3	4.7	0.6
	1344 μm ($8.3Z_R$)	0.8	6.0	1.4
$1.5Z_R$ (212 μm)	270 μm ($0.2Z_R$)	0.0	4.8	0.1
	1173 μm ($6.6Z_R$)	0.5	6.6	1.8
	1515 μm ($9Z_R$)	0.8	7.1	2.0
$2Z_R$ (282 μm)	311 μm ($0.0Z_R$)	0.0	4.4	0.1
	1312 μm ($7.1Z_R$)	0.6	5.5	1.4
	1597 μm ($9.1Z_R$)	0.8	5.7	1.7

$$E_z(x,y,t) = E_0\left[\frac{W_0}{W(x)}\right]^{1/2}\exp\left[-\frac{(y-y_c)^2}{W^2(x)}\right]\mathrm{env}(\zeta) \times \cos\left[\frac{k(y-y_c)^2}{2R(x)} - \frac{1}{2}\phi(x) + k_0 x - \omega_0 t\right], \quad (1)$$

where the width of the pulse is

$$W(x) = W_0\sqrt{1+(x-x_f)^2/Z_R^2}, \quad (2)$$

x is the position of the pulse along its direction of propagation, W_0 is the width at the location of the vacuum focus x_f, $Z_R=\pi W_0^2/\lambda_0$ is the Rayleigh length, λ_0 is the pulse wavelength [k_0 and ω_0 are the wave vector and (angular) frequency of the pulse], E_0 is the field amplitude, $R(x)=x-x_f+Z_R^2/(x-x_f)$, and $\phi(x)=\tan^{-1}[(x-x_f)/Z_R]$. The pulse longitudinal envelope profile is given by the function env(ζ), where $\zeta=x-c(t-t_0)$ and t_0 is the turn on time of the pulse. We use a half sine envelope function for all simulation results reported here,

$$\mathrm{env}(\zeta) = \sin\left(\frac{\pi\zeta}{L}\right)I_{[x-L,x]}(\zeta),$$

where L is the full longitudinal length of the pulse [$L/2$ is the full width at half-maximum (FWHM)] and $I_{[a,b]}(x)$ is the indicator function, $I_{[a,b]}(x)$ is equal to unity for $x\in[a,b]$ and zero otherwise.

The laser pulses of the type given by Eq. (1) were always launched in a vacuum region with W_0 and x_f given as input parameters.

One could neglect the ramp and launch the laser pulse such that it would have its focus at the entrance of the plasma channel if the ramp were not present. However, the problem with this approach is that the pulse does not propagate only in vacuum until it reaches the channel entrance but also moves through the plasma density ramp. The interaction of the pulse with the plasma in the ramp leads to a waist location different from the location of the channel entrance. The results of our simulations confirm that the energy loss due to *leakage* out of the channel increases when the actual waist location is shifted from the top of the density ramp. This can happen when the density ramp length is of the same order as the Rayleigh length, and some channel formation has occurred within the ramp. In Sec. II B, we consider the interaction of a pulse with the plasma in the ramp and show how the parameters of the laser pulse at launch have to be chosen for optimal guiding. This is an important effect that should be taken into account when designing such experiments. These results are also confirmed by the PIC simulations.

We also track the evolution of the laser spot size inside the channel using a power spectral diagnostic (it is described in the Appendix). When the laser pulse vacuum parameters are chosen to match the plasma channel, assuming the effect of the plasma density ramp is negligible, strong betatron oscillations of the spot size are observed when the pulse propagates in the channel. However, if we take into account the parameters of the ramp when selecting the laser pulse launch parameters, the spot size oscillations in the channel are much smaller leading to efficient coupling to the channel.

In Sec. II A, we specify the plasma density profile (both for the ramp and the channel) and the rest of the simulation setup, including numerical parameters. We derive laser pulse launch parameters for optimal guiding in the plasma channels considered here (taking into account the evolution of the pulse in the ramp) in Sec. II B. Results from VORPAL PIC simulations are presented and discussed in Sec. II B on spot size evolution and in Sec. II C on pump depletion and leakage out of the channel.

A. Preformed plasma channel profile and simulation parameters

In all simulations, the laser pulse is taken to be linearly polarized along the transverse z direction, with an amplitude variation that is longitudinally a half-sine pulse as given by Eq. (1). We note that Eq. (1) describes a solution of the paraxial Helmholtz wave equation in 2D. The laser pulse used in our simulations was chosen to have wavelength $\lambda_0=0.8$ μm and normalized amplitude $a_0=eA_0m_ec^2=0.7$ (A_0 is the amplitude of the vector potential), leading to a peak intensity of 10^{18} W/cm^2. The pulse FWHM was set to 50 fs (full length $L_0=30$ μm for the half sine pulse envelope) and the vacuum waist size to $W_0=6$ μm. The Rayleigh length is $Z_R=141$ μm. The laser pulse is launched into a 30 μm vacuum region followed by a preionized density ramp of length Z_R, $3Z_R/2$, or $2Z_R$. The shape of the plasma density ramp is given by

$$n(x,y) = \begin{cases} 0, & x \le x_0 \\ \frac{1}{2}\left[1-\cos\left(\frac{\pi(x-x_0)}{L_r}\right)\right]\left[n_0+\Delta n\left(\frac{y-y_0}{r_0}\right)^2\right], & x_0 \le x \le x_0+L_r,\ |y-y_0|\le 2r_0 \\ n_0+\Delta n\left(\frac{y-y_0}{r_0}\right)^2, & x \ge x_0+L_r,\ |y-y_0|\le 2r_0 \\ 0, & x \ge x_0,\ |y-y_0|>2r_0 \end{cases} \quad (3)$$

where L_r is the length of the ramp, and the peak density $n_0=1.238\times10^{24}$ m^{-3}, which corresponds to a plasma wavelength of 30 μm and to a plasma frequency of $\omega_p=6.297\times10^{13}$ s^{-1}. The plasma density is matched to the pulse length to produce the maximum plasma wave response, as used for LWFA.[11] The density ramp is followed by a preformed (preionized) plasma channel. The channel is modeled by a transverse parabolic density profile.

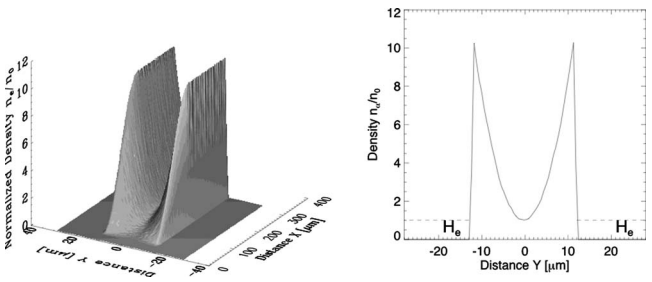

FIG. 1. The surface plot shows the normalized electron density profile for the parabolic channel used in our simulations. The density is normalized with respect to n_0. The channel walls extend up to $|y|=2r_0=12$ μm ($y_0=0$ in all simulations). The line plot shows the transverse density profiles for the electrons and neutral He gas. The He gas density is located only on the sides of the plasma channel. There is no He density in the domain of the preionized plasma given by Eq. (3). The He density is ramped from 0 to $n_{\mathrm{He}}=n_0$ with the same longitudinal profile as the plasma channel. Once it reaches n_0, it is held constant. For the simulations without tunneling ionization, the neutral gas at the sides of the channel was replaced with vacuum.

The parabolic channel profile can guide a Gaussian beam with $W_0=r_0$ when the density channel depth is equal to the critical depth, $\Delta n=\Delta n_c$, where $\Delta n_c=(\pi r_e r_0^2)^{-1}$, and r_e is the classical electron radius.[1,12] For $r_0=6$ μm, we have $\Delta n_c=3.13\times10^{24}$ m^{-3}. This is the theoretical value for guiding in the absence of nonlinearities. Figure 1 illustrates the electron density profile for the plasma channel used in our simulations. The density is normalized with respect to the density at the bottom of the channel n_0.

The simulation region has size $L_x\times L_y=320$ μm $\times 58$ μm for the Z_R and $1.5Z_R$ long density ramp cases and $L_x\times L_y=500$ μm $\times 121$ μm for the $2Z_R$ long ramp case. In all cases the x-cell size is $dx=5.0\times10^{-8}$ m, which corresponds to 16 cells per laser wavelength and y-cell size $dy=15.0\times10^{-8}$ m. The time step is chosen to satisfy the Courant condition, $dt=1.358\times10^{-16}$ s. We use five particles per cell at full density (n_0) and a moving window algorithm, which moves the simulation box at the speed of light following the propagation of the laser pulse.

B. Optimal laser pulse parameters in the presence of a channel ramp

Before we discuss results from the PIC simulations, we consider here how to launch a laser pulse in vacuum for optimal coupling to a plasma channel preceded by a plasma density ramp. We apply the source-dependent expansion (SDE),[1,7,8] and references therein, to the paraxial wave equation to analyze the evolution of the laser pulse in the plasma density profile given by Eq. (3). Using the SDE method, we obtain the following equation for the laser spot size evolution,

$$\frac{d^2W}{dx^2}=\frac{4}{k_0^2W^3}-\frac{\Delta n}{n_0}f(x)\frac{W}{r_0^2} \tag{4}$$

in the plasma density given by Eq. (3), where

$$f(x)=\begin{cases}0, & x\leqslant x_0\\ \dfrac{1}{2}\left[1-\cos\left(\dfrac{\pi(x-x_0)}{L_r}\right)\right], & x_0\leqslant x\leqslant x_0+L_r\\ 1, & x_0+L_r\leqslant x\end{cases}$$

is from the longitudinal profile of the plasma density. The conditions for the optimal coupling of a laser pulse to the plasma channel are

$$W(x_0+L_r)=r_0,\quad \frac{dW}{dx}(x_0+L_r)=0. \tag{5}$$

The problem is to determine the laser pulse parameters at the location of its launch: $x_l<x_0$ (which is in vacuum), which will satisfy the conditions for optimal coupling when the pulse reaches the entrance of the plasma channel. In the PIC simulations here, we launch the laser pulse in vacuum using Eq. (1) with W_0 and x_f as input parameters. If the presence of the plasma density ramp is neglected by setting $f(x)=0$ for $x<x_0+L_r$, then selecting the input parameters W_0 and x_f is directly given by $W_0=r_0$ and $x_f=x_0+L_r$ (the position of the plasma channel entrance). But this approach leads to inefficient coupling to the channel, as we show below, since the propagation in the plasma ramp changes the actual pulse focus location (it is no longer at the entrance of the channel) and the minimum spot size.

To determine the correct input parameters W_0 and x_f, when launching a laser pulse in vacuum, we solve Eq. (4) numerically with initial conditions given by Eq. (5). This solution allows us to determine $W(x_l)$ and $dW/dx(x_l)$ at the position of the laser pulse launch, i.e., we solve Eq. (4) backwards in space to find the values for the spot size and its derivative at x_l. Then, the correct (vacuum) input values for W_0 and x_f can be expressed as functions of $W(x_l)$ and $dW/dx(x_l)$.

We implemented Stoermer's rule[13] to solve numerically Eq. (4) in its reduced units representation,

$$\frac{d^2R}{d\chi^2}=\frac{1}{R^3}\left[1-\frac{\Delta n}{\Delta n_c}f(\chi)R^4\right], \tag{6}$$

where $R(x)=W(x)/r_0$, $\chi=x/Z_R$, and the initial conditions are correspondingly rescaled. Using the numerical solution of Eq. (6) at the laser pulse launch position,

$$R_l=R(\chi_l),\quad \left(\frac{dR}{d\chi}\right)_l=\left(\frac{dR}{d\chi}\right)(\chi_l),$$

where $\chi_l=x_l/Z_R$, we can determine the correct (vacuum) laser pulse parameter W_0 from

$$W_0=r_0g_l \tag{7}$$

and x_f from

$$x_f=x_l+Z_Rg_l\sqrt{R_l^2-g_l^2}, \tag{8}$$

where

$$g_l=R_l/\sqrt{1+R_l^2\left(\frac{dR}{d\chi}\right)_l^2}.$$

The following three examples demonstrate the effect of the plasma density ramp on the values of the laser pulse launch parameters. We also compare the results from these three cases to VORPAL PIC simulations.

In the first case, the length of the ramp is $L_r=Z_R$, in the second $1.5Z_R$, and in the third $2Z_R$ Rayleigh lengths. We solve Eq. (7) numerically using a similar setup as in the corresponding PIC simulations. The laser pulse is launched with its origin (the center of the pulse) located at $x_l=-15$ μm. This value is chosen specifically for the laser pulse parameters we use in the PIC simulations as described in the previous subsection. The choice is made in order to start launching the front of the pulse at the left boundary of the VORPAL simulations box that is at $x=0$ (at the beginning of a simulation and before the moving window is turned on). The pulse is then propagated in vacuum until it is completely in the simulation box before it starts to interact with the plasma density ramp. Since the pulse length is approximately 30 μm, the plasma ramp starts at $x_0=30$ μm.

From the numerical solution of Eq. (6) and with the help of Eqs. (7) and (8), we obtain the values $W_0=6.1$ μm and $x_f=100$ μm in the case of one Rayleigh length long ramp. These values are of considerable importance and interest. They indicate that we need to launch a laser pulse in vacuum using Eq. (1) with input values for the waist $W_0>r_0=6$ μm larger than the channel radius and with a focal location $x_f<x_0+L_r$ before the top of the ramp in order to obtain the actual waist of the pulse to be at the entrance of the plasma channel and equal to its radius. This shows that even in the case of one Rayleigh length long ramp, its effect is significant. If there were no ramp and the channel starts again at $x_0+Z_R\approx 171$ μm, then we use as input for the pump launcher the values $W_0=6$ μm and $x_f=171$ μm. However, due to the presence of the Z_R long plasma density ramp, we have to launch the laser pulse with $W_0=6.1$ μm and $x_f=100.0$ μm for the real waist location to be at $x_0+Z_R\approx 171$ μm and the realized waist size approximately equal to $r_0=6$ μm. Notice that to obtain this optimal coupling in the presence of the ramp, the input value of W_0 has to increase by only 2% but the location of the pulse focus x_f has to decrease by more than 40% from the vacuum (no plasma ramp) case value.

When the length of the plasma density ramp increases to $1.5Z_R$, a laser pulse launched in vacuum with $W_0=6.3$ μm and $x_f=134$ μm will couple optimally to the plasma channel. In this case, W_0 increases by 5% and x_f decreases by approximately 45%. Finally, for the $L_r=2Z_R$ long plasma ramp, the laser pulse has to be launched with $W_0=6.6$ μm, a 10% increase relative to the channel radius, and $x_f=166$ μm, a 47% decrease from the location of the plasma channel entrance (the top of the plasma density ramp).

Figure 2 shows the laser spot size as it propagates inside the plasma where the ramp lengths are increased from Z_R to $1.5Z_R$, and finally to $2Z_R$. The top plot on Fig. 2 is for the Z_R long ramp. The open squares are for the simulation case with the vacuum focus chosen at the top of the ramp (the lines through the symbols are to serve as guides to the eye) and the vacuum waist input parameter is set to $r_0=6$ μm. There are large-amplitude laser spot size oscillations. We will see

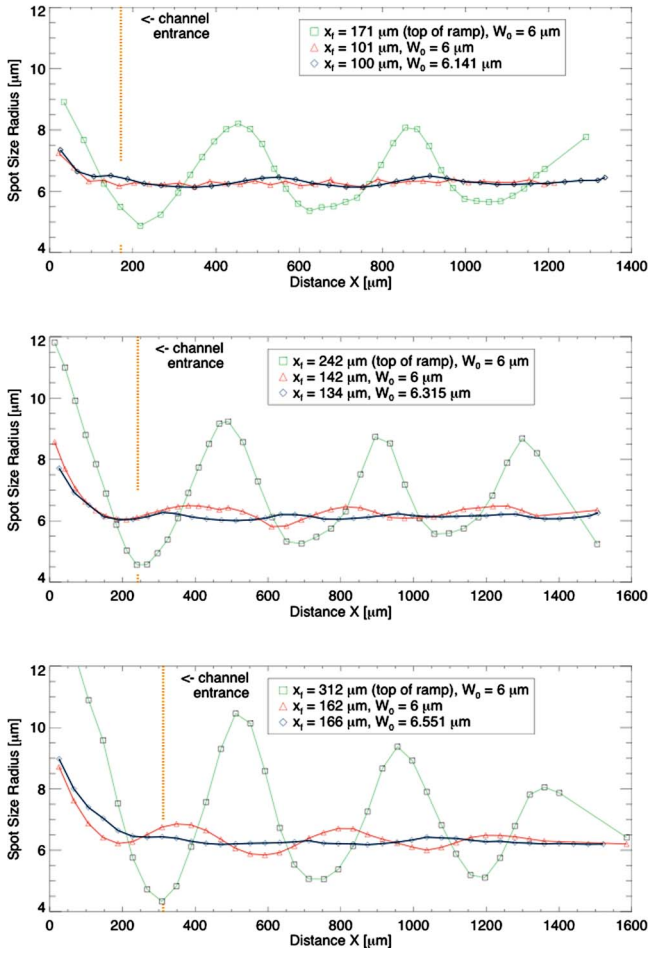

FIG. 2. (Color online) The behavior of the laser pulse spot size as a function of propagation distance for ramp lengths of Z_R (top plot), $1.5Z_R$ (middle), and $2Z_R$ (bottom) shows large amplitude oscillation when the pulse is vacuum focused at the top of the plasma channel and its waist is set to the channel radius. In this case, the pulse is overfocused at the entrance of the channel. Moving the pulse focus in the plasma density ramp in order to move its waist location close to the channel entrance (but keeping $W_0=r_0$) decreases the spot size oscillation for shorter ramp length. But when the ramp length increases, the spot size oscillations increase showing the importance of selecting optimal values for both x_f and W_0.

that these oscillations lead to increased pump depletion and leakage. Moreover, the pulse is overfocused at the entrance of the channel.

The second case we simulated was with the vacuum waist set again to r_0, but this time we set the vacuum focus in the ramp at $x_f=101$ μm in an attempt to compensate for the overfocusing seen in the previous simulation. The results from this simulation are plotted with the open triangles. Now, the spot size is slightly inside the channel (small underfocusing). More importantly, the pulse is very well coupled to the channel and its spot size stays approximately constant (the line through the triangles shows very small variations, particularly when compared to the previous case). Finally, we show with the open diamond symbols the result from the simulation with the optimal parameters obtained from the numerical solution of Eq. (4) with the boundary conditions (5). In this case, the waist is at the channel entrance and again the spot size stays approximately constant when the pulse propagates in the channel. The results from

the previous simulation case are very close to the optimal coupling case since the waist sized differed by only 2% and the vacuum focus locations by 1%.

The middle plot is for the $1.5Z_R$ ramp. The simulation with the vacuum focus at the channel entrance and waist equal to r_0 is even more overfocused at the top of the ramp (compared to the corresponding case with one Z_R long ramp). The laser pulse also shows large spot size oscillations. Here, we again moved the vacuum focus in the ramp (to $x_f = 142$ μm) and kept $W_0 = r_0$. This simulation now also shows spot size oscillations even larger than in the previous case. The simulation with the optimal parameters shows a clear improvement even from the simulation with $x_f = 142$ μm and $W_0 = r_0$. The reason is that for $W_0 = r_0$, the vacuum waist differs from the optimal vacuum waist by 5% and the vacuum focus location is no longer as close to the optimal vacuum focus location as in the top plot. The difference is even larger in the $2Z_R$-long ramp case shown in the bottom plot. Here, even the case with the vacuum focus in the ramp and with $W_0 = r_0$ shows large spot size oscillations compared to the simulation with the optimal vacuum focus location and the waist chosen from the solution of Eqs. (4) and (5). The reason is that the optimal value of $W_0 = 6.6$ μm is now close to 10% larger than r_0.

Recently, Wu *et al.*[14] considered effective coupling in funnel-mouthed plasma channels. They found from their simulations that the coupling efficiency to a channel increases when the vacuum focus is placed in the plasma density ramp and its vacuum waist is chosen to be larger than the channel radius. Our main contribution here is that we propose an explanation for this behavior and how to predict the optimal values for the vacuum focus and waist given the plasma ramp length and channel radius.

In the next section, we will see how the mismatch degrades the energy coupling between the pulse and channel.

C. Energy loss inside a plasma channel

A laser pulse propagating inside a plasma will gradually lose energy, reducing the accelerating fields of the LWFA and the maximum energy of trapped electrons. In our study, two important energy-loss mechanisms are considered: pump depletion and energy leakage transversely through the channel walls. The channel interior is defined to extend over the transverse range $-2r_0 \leqslant y \leqslant 2r_0$. Here, energy loss as the pulse enters into the channel and after a specific number of Rayleigh lengths of propagation is calculated using the power spectral diagnostics (PSD) described in the Appendix. The PSD diagnostic is calculated in a postprocessing mode after field data dumps are generated. The freedom to select a spatial region for FFT allows us to calculate the power spectral density in any subregion of the simulation box. For example, if we select the subregion that contains the pulse, we will obtain its power spectrum. If we select the region of the wake (behind the pulse) and the appropriate electric field component, we can calculate the power spectrum of the excited plasma wave.

We estimate the pump depletion in the channel by calculating first the power spectrum in the channel over the domain of the pulse $[x_{\min}, x_{\max}] \times [N_0 \Delta t, N_1 \Delta t]$ (where $N_1 - N_0 = 128$) and then integrating the calculated PSD over the transverse domain $-y_{\min} \leqslant y \leqslant y_{\max}$. Second, we calculate the power spectrum of the same pulse in vacuum at its focal location using spatial and temporal domains with the same sizes. The values of $y_{\min}$ and $y_{\max}$ were chosen to cover the full transverse width of the simulation region when calculating the total spectral power from E_z. We sample in time once per time step to obtain approximately the same number of data points in a pulse period as the number of spatial points over a pulse wavelength.

Pump depletion is calculated as

$$P_{\mathrm{pd}} = \frac{(\mathrm{PSD}_{\mathrm{vac}} - \mathrm{PSD}_{Ny})}{\mathrm{PSD}_{\mathrm{vac}}} \times 100, \tag{9}$$

where $\mathrm{PSD}_{\mathrm{vac}}$ is the power spectral density for the case of a pulse in vacuum when it is at focus and PSD_{Ny} is the density over the transverse region of the simulation domain when the pulse propagates in plasma. The results for the pump depletion for the simulation with the vacuum focus at the top of the ramp and $W_0 = r_0$ (the mismatched case) are shown in Table I and in Table II for the optimally matched case.

It is of interest to compare the pump depletion data from the PIC simulations to theoretical results.[15] Note, however, that the theory is for a 1D system, a square profile laser pulse, and constant plasma density. The pump depletion length, L_{pd}, that it predicts for a pulse with linear polarization and $a_0 \leqslant 1$ is

$$L_{\mathrm{pd}} \simeq \frac{2}{a_0^2} (\omega_0/\omega_p)^2 \lambda_p.$$

Since $2\lambda_p/a_0^2 \simeq Z_R$ and $(\omega_0/\omega_p)^2 \gg 1$ for the pulse and plasma parameters we consider here, we approximate the pump depletion to increase linearly with the propagation distance over the distances we simulated. Thus, for propagation distances of

$$Z_R(3.3, 8.3, 6.6, 9.0, 7.1, 9.1)$$

in the channel, we obtain the corresponding values for the pump depletion in percents,

$$(0.3, 0.7, 0.5, 0.7, 0.6, 0.7).$$

These can now be compared to the pump depletion values calculated from the PIC simulations data using the power spectral diagnostic. The first two values of P_{pd} of 0.3 and 0.8% are for pulse propagation of $3.3Z_R$ and $8.3Z_R$ in the channel. They should be compared to the pump depletion results from the simulation with a Z_R-long ramp given in Table I, 0.4 and 0.9%, for the mismatched case and in Table II, 0.3 and 0.8% for the optimally matched case. Here, the unmatched case shows larger pump depletion than the optimally matched case and the result from the 1D theory. The greater pump depletion in the unmatched case is due to the spot size oscillations. When the pulse is not matched to the channel and its spot size oscillates, the energy deposition per unit length is always greater than for the matched (nonoscillating spot size) case due to the nonlinear dependence of the wake field on the laser pulse field. The optimally matched

case agrees well with the result from the 1D theory (within the precision considered here).

For the simulation with a $1.5Z_R$-long ramp, the pump depletion for the unmatched case is 0.8 and 1.1% for propagation distances of $6.6Z_R$ and $9.0Z_R$ in the channel. The pump depletion values for the same propagation distances in the optimally matched case are 0.6 and 0.9%, respectively, or about 30% smaller. These values are again in good agreement with the 0.5 and 0.7% from the 1D theory (although the simulations show larger pump depletion than the theory).

As we saw from the spot size oscillation plots, the unmatched simulation with a $2Z_R$-long ramp deviates the most from the corresponding optimally matched case. This is also reflected in the results for the pump depletion. In the unmatched simulations with $2Z_R$ ramp, the pump depletion is 1.4 and 1.3% for propagation distances of $7.1Z_R$ and $9.1Z_R$ in the ramp. These values are about 100% larger than the corresponding P_{pd} values from the 1D theory. The pump depletion results from the optimally matched case are again in good agreement with the 1D theory. However, in the unmatched simulations, the 1.3% pump depletion is for larger propagation distance than the 1.4% value. We expect that this increase of 0.1% in P_{pd} could be due to two effects. First this value is within the error of the pump depletion when estimated with the PSD diagnostic. We did three different simulations with the same propagation distance but on a different number of processes (causing different random number sequences to be used by each process and thus loading particles at different cell positions). The pump depletion values obtained from these three runs after $9.1Z_R$ propagation in the channel are within 0.1% of the 1.3% value in Table II. The second effect could lead to less pump depletion for some (increasing) pulse propagation distances. This effect is caused by electromagnetic field reflections from the transverse simulation boundaries. We used "perfect conductor" boundary conditions at the transverse boundaries of the simulation box. It was shown by Clark and Milchberg[16] that the modes in the channel consist of one inward-directed and one outward-directed conics. The outward one is associated with power leaked out of the channel. Once part of this mode is outside of the plasma channel, it will propagate with a group velocity that is greater than the group velocity of the pulse inside of the channel and at some angle to the axis of the channel. This mode will eventually reflect from the "perfect conductor" boundary and will return toward the channel. If a measurement is made when this leaked mode catches with the pump in the channel, the pump depletion could show a larger value compared to a measurement taken at an earlier time. This effect is an artifact of the simulation setup. It indicates that for large propagation distances, one has to use either a very wide simulation box or absorbing boundary conditions, e.g., perfectly matched layer (PML)[17] ones. There are uniaxial PML[18] boundary conditions implemented in VORPAL. PMLs are specifically designed to absorb electromagnetic waves and improve the simulations of unbounded electromagnetic problems. We will consider the effect of using PML boundaries on pump depletion over long propagation distances ($\geqslant 2Z_R$) in a separate study (we did several preliminary simulations with PMLs for shorter propagation distances, less than $2Z_R$, and the results on pump depletion and leakage are essentially the same as the results with perfect conductor boundaries).

The leakage out of the channel was calculated similarly to pump depletion except that the sum over lines with $y=\mathrm{const}$ was limited to two regions that extend transversely over $-r_0 \leqslant y \leqslant r_0$ and $-2r_0 \leqslant y \leqslant 2r_0$. The first region contains the channel interior within the limits for optimal pulse coupling. The second region extends over the whole transverse domain of the unperturbed plasma density. The calculated total power spectrum is again compared to the total power spectrum for the same pulse in vacuum at its focus location and subtracted from the pump depletion calculated for the same propagation length. Energy leakage outside of the channel (as we define it for the purpose of pulse guiding) is calculated as

$$P_{\mathrm{lk}} = \frac{(\mathrm{PSD}_{Ny} - \mathrm{PSD}_{\mathrm{ch}})}{\mathrm{PSD}_{\mathrm{vac}}} \times 100, \tag{10}$$

where $\mathrm{PSD}_{\mathrm{ch}}$ is the density in the plasma channel over the first or second regions. The results for leakage out of the first region are shown in the "$P_{\mathrm{lk}}^{[-r_0,r_0]}(\%)$" column and outside of the whole plasma density region in the "$P_{\mathrm{lk}}^{[-2r_0,2r_0]}(\%)$" column of Table I for the unmatched case and in Table II for the optimally matched one.

Due to the laser spot oscillations in the unmatched case, higher-order modes will be excited in the channel. The higher-order modes have a much greater leakage rate than the fundamental mode leading to much faster power leakage out of the channel compared to the optimally matched case.[7,16] This is supported by the leakage data obtained from our PIC simulations. In particular, the leakage outside of the whole plasma channel region for the unmatched case is at least twice as large as for the matched case for the same propagation distances. Moreover, as expected, this ratio increases when increasing the propagation distance and the "degree" of mismatch from the optimal matching. The leakage is more than five times larger for the unmatched simulation with a $2Z_R$-long ramp and propagation distance of $9.1Z_R$ in the channel when compared to the optimally matched case at the same parameters.

The oscillations of the spot size around the matched channel radius r_0 that we observed in Fig. 2 for the unmatched simulation cases are also evident in the leakage outside of the two transverse regions. For example, in the simulations with a $1.5Z_R$-long ramp, the leakage when the pulse has propagated $6.6Z_R$ inside the channel is larger (8.8% for the first transverse region and 5.1% for the second one) compared to the leakage (5.3% and 4.1%, respectively, for the two transverse regions) at the longer, $9.1Z_R$ propagation distance. The spot size for the $6.6Z_R$ propagation distance is approximately 6.0 μm while for propagation of $9.1Z_R$ the spot size is 5.2 μm. For the optimally matched simulations, the leakage decreases with propagation distance in the channel for both transverse regions that we calculated.

It is also of importance to understand how the leakage values obtained from the numerical diagnostic compare to available theoretical calculations. The most relevant theory

we can currently compare to was developed by Volfbeyn *et al.*[7] They used the WKB approximation in a 1D slab geometry to derive an estimation for the decrease of the power in *only* the fundamental mode due to leakage outside of the plasma channel

$$P \simeq P_0 \exp(-T_\perp x/Z_p),$$

where P_0 is the initial mode power at $x=0$ (which we take here relative to the location of the channel entrance), $Z_p = \pi Z_R$, and

$$T_\perp \simeq (R_x + \sqrt{R_x^2 - 1})\exp(-R_x\sqrt{R_x^2 - 1}),$$

with $R_x = \sqrt{2} r_{\mathrm{ch}}/r_0$ (r_{ch} the transverse radius of the plasma density channel). For the simulations here, $r_{\mathrm{ch}} = 2r_0$ and hence $R_x = 2\sqrt{2}$. The leakage (in percents) outside of the plasma density region for the channel we consider is estimated by

$$P_{\mathrm{lk}}^{[-2r_0, 2r_0]} \simeq 100 \times [1 - \exp(-T_\perp x/Z_p)]. \quad (11)$$

Note that the result given by Eq. (11) is only for the leakage of the fundamental mode. However, pulse width oscillations indicate the excitation of higher-order modes in the channel. These modes have a much larger leakage rate than the rate for the fundamental mode.[7] The numerical diagnostic for estimating the leakage includes the contributions from the higher-order modes as well as the effect of the ramp. The theory did not consider leakage from channels with ramps.

The values for the leakage outside of the plasma channel density calculated from Eq. (11) for the same propagation distances, Z_R (3.3, 8.3, 6.6, 9.0, 7.1, 9.1), as in the case of pump depletion, are (0.3, 0.8, 0.6, 0.9, 0.7, 0.9)%. Again, the first two values are for the run with a Z_R-long ramp, the next two are for the run with $1.5Z_R$, and the final two are for the case with a $2Z_R$-long ramp. The corresponding values for the leakage when the pulse is not optimally matched to the channel are (1.7, 2.8, 5.3, 4.1, 6.6, 9.1)% (from Table I). These leakage values are several times larger than those estimated from this theory. The largest difference is for the run with a ramp length of $2Z_R$ and propagation length of $9.1Z_R$ in the channel. The significant leakage increase when the pulse is mismatched is consistent with the behavior that the excited higher-order modes will quickly lose their power via leakage.[7]

In comparison to the unmatched runs, the leakage values (0.6, 1.4, 1.8, 2.0, 1.4, 1.7)% (from Table II) for the simulations with optimally matched pulse parameters are from two to more than five times smaller and in better agreement with the values from the theory. However, even for the runs with the optimally matched pulse parameters, the leakage values are larger than the estimates from this theory. The largest difference is by a factor of 3 and the smallest by 57%. This behavior is expected. The theoretical leakage values are only from the fundamental mode while the simulations include the leakage from the higher-order modes too. The leakage is also very sensitive to the initial conditions: the simulations include a ramp while the theory did not take into account the effect of the ramp. Nevertheless, the results for leakage from the numerical diagnostic are about the same order of magnitude as the results from the theory. This indicates that the diagnostic is a useful tool to estimate leakage in the process of finding the optimal parameter regime for coupling a pulse to a laser channel.

The results on pump depletion and leakage from the simulations and the related theoretical results show that for ramp lengths relevant to LWFA experiments, appropriate focusing of the laser pulse can be used to provide matched coupling into the channel with minimal subsequent depletion, leakage, and spot size oscillations.

III. MODELING OF IONIZATION EFFECTS

The implementation of field-induced tunneling ionization physics in VORPAL uses the IONPACK library (IONPACK is being developed at Tech-X Corp. and is now a part of the TxPhysics[19] software library) to calculate tunneling ionization probability rates[20–24] for atoms and ions. We use this computational capability in VORPAL to study how field ionization processes affect laser pulse propagation in channels when there is He gas on the sides of the plasma region (ramp and channel). Finally, we present results from exploratory runs on the effect of field ionization of an He gas tail in front of the plasma ramp.

We model neutral gas with a profile relevant to hydrodynamic channel formation experiments.[5,16] In such experiments, precursor laser pulse(s) ionize and heat a filament of plasma from a gas jet. Expansion of this plasma into the surrounding neutral gas then drives a shock wave, resulting in a low density on axis, and high density off axis. Outside the shock front, neutral gas remains as shown in the transverse density profile of Fig. 1.

The value of the neutral gas density after the ramp was chosen to be $n_{\mathrm{He}} = 1.238 \times 10^{24}\ \mathrm{m}^{-3}$ equal to the electron density at the channel center. The gas density is only in the region outside of the plasma channel. It is increased from zero to n_{He} in the ramp region using the same longitudinal ramp profile as the one given in Eq. (3). The ratio of central channel plasma density to neutral density (outside of the channel) is similar to recent experiments,[5,16] though for reasons of computational cost, the channel walls are higher and narrower in the simulations.

Gas atoms can be ionized by the wings of the pulse (if its field is sufficiently strong) leading to additional effects in the pump depletion and leakage that could affect the pulse guiding. In all other respects, the plasma and laser pulse parameters are chosen to be the same as for the simulations discussed in Sec. II. Again, we simulate two cases. The first is with the vacuum focus located at the entrance of the channel (and the vacuum waist set to r_0). The second is with the optimal matching parameters as in the preionized channel runs.

We consider first the evolution of the laser pulse spot size. Its behavior along the direction of propagation in the channel is shown in Fig. 3 for the different simulation cases.

The evolution of the spot size is similar to the corresponding simulation cases without He (and no tunneling ionization) shown in Fig. 2. This shows that up to these pulse propagation distances and densities of He outside of the

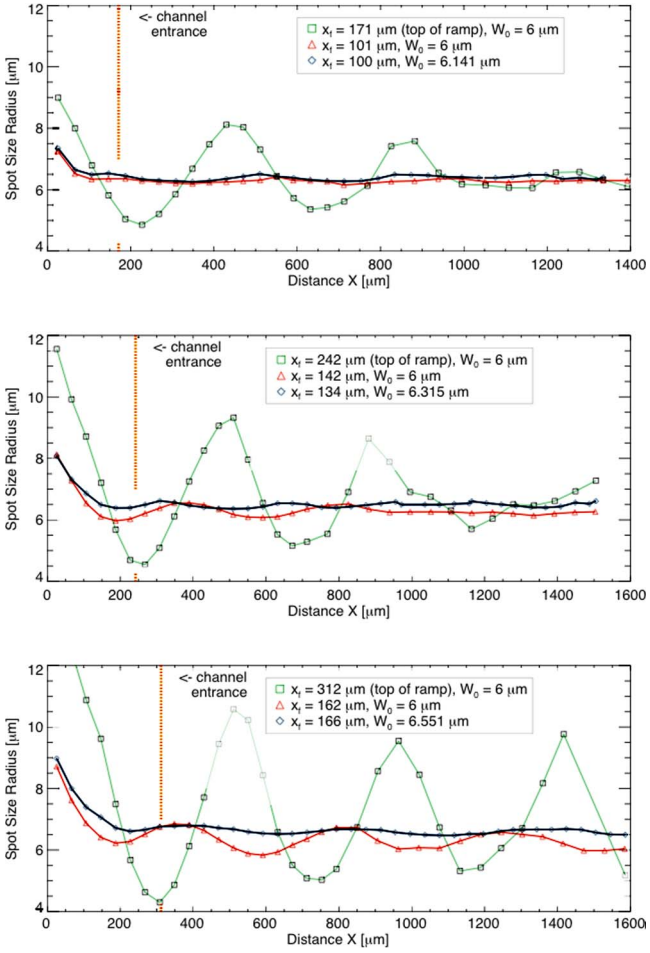

FIG. 3. (Color online) For the simulations with He gas outside of the plasma channel, the evolution of the laser pulse spot size as a function of propagation distance for ramp lengths of Z_R (top plot), $1.5Z_R$ (middle), and $2Z_R$ (bottom) shows large-amplitude oscillations when the pulse is vacuum focused at the top of the plasma channel and its waist is set to the channel radius. This behavior is similar to the spot size evolution in the simulations without the He gas, shown in Fig. 2. Even in the presence of neutral gas, the optimal focus location and waist parameters obtained in Sec. II show almost no spot size oscillations.

given channels, the field ionization did not affect the spot size significantly. Moreover, using the optimal matching vacuum focus locations and waist sizes that we obtained in Sec. II (for the different ramp lengths in preionized channels) when there is He outside of the channels, the spot size oscillations are suppressed again. This also indicates that the presence of such He densities outside of the channel does not lead to a significant effect on the spot size evolution. Hence, for these cases, we can still use the optimal pulse matching parameters obtained from a model that includes only a preionized plasma density profile and obtain pulse guiding that is approximately optimal. The behavior of the spot size for the runs with $W_0=r_0$ and the vacuum focus placed in the ramp are also similar. The results in Fig. 3 show that oscillations in the spot size for these simulations grow when increasing the ramp length. This is expected since the waist size stays constant, while for optimal coupling the waist has to increase when the ramp length is increased.

To understand how field ionization affects the laser

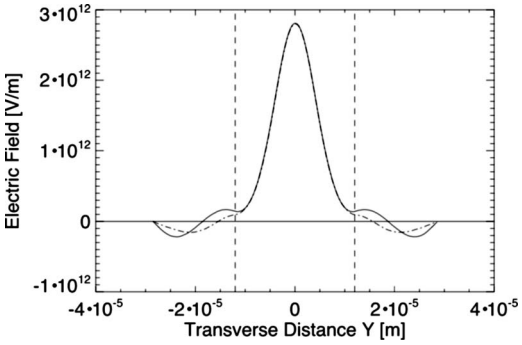

FIG. 4. The effect of tunnel ionizing He on the laser pulse E field leads to a decrease of the field amplitude (and intensity) in the He gas regions where the field is strong enough to ionize He atoms and He^+ ions. This is demonstrated when comparing lineouts of the laser pulse electric field (its z component for the linear polarization we study here) along a line in the transverse (y) direction from a simulation without the He gas (solid line) and from another run with the gas (solid-dashed line). These results are for the line x=const through the maximum field amplitude, after $8Z_R$ length of propagation in the channel. The ramp is one Rayleigh length long. The pulse focus is at the top of the ramp (nonoptimally matched case). The vertical dotted lines mark the limits of the plasma channel. For the same spatial positions, the amplitude of the field that is leaked outside of the channel is smaller for the run with tunneling ionization compared to the amplitude for the run without the He gas.

pulse, we plot in Fig. 4 the pulse electric field along the transverse direction from one of the simulations. When tunneling ionization is present, the electric field leaked outside of the channel depletes, particularly in the domain where the field has its maximum amplitude for the simulation without He gas. Figure 5 shows a snapshot of He^+ and He^{++} ions. The location of stripes seen in Fig. 5 is consistent with the domains where the amplitude of the laser electric field shown in Fig. 4 is close to maximum values in the regions with He gas.

Using the PSD diagnostics, we have calculated the pump depletion and leakage at the same locations in the plasma density as we did in Sec. II for the simulations without He. The results in the presence of neutral He outside the channel walls differ only by fractions of a percent from the idealized case of complete ionization; hence, we do not present these results in detail.

Variation of helium density was not simulated because the effect was negligible, and hence small variation of the helium density would not produce a significant change in the guiding performance, while large changes would be outside the range relevant to experiments.

Apart from studying the effect of field ionization of He gas on the sides of the plasma, we also did several runs to explore how field ionization of the He gas tail in front of the plasma affects the coupling of laser pulses to preformed plasma channels. In part of the experiments, the gas is fully ionized when the plasma channels are produced so the pulse does not interact with the gas before reaching the plasma ramp. However, there are experimental cases in which a low-density gas tail may exist before the plasma ramp.[5,25]

For example, in capillary experiments the arc might not fully ionize the jet coming out of the end of the capillary and a low-density gas tail may exist. This tail could be long up to

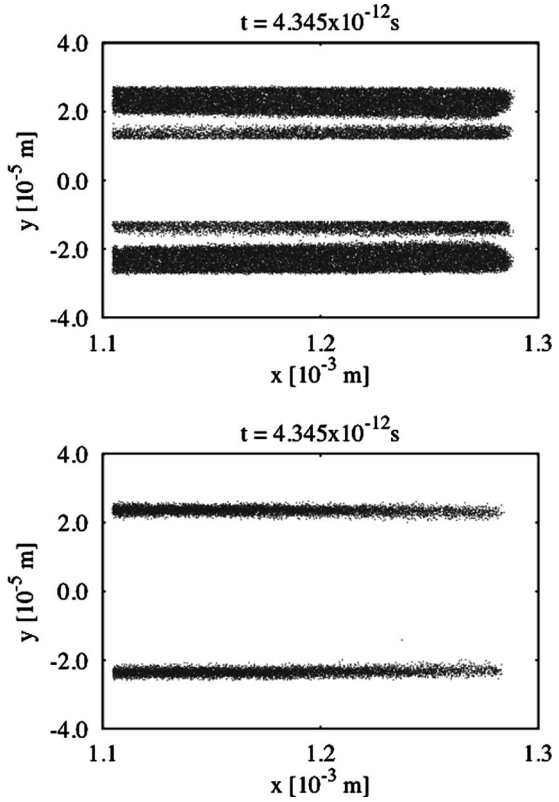

FIG. 5. The particle plots of He^+ (top) and He^{++} (bottom) ions confirm that the tunneling ionization processes are localized in the domain of largest field amplitudes outside of the channel (compare the position of the ionization particle stripes to the positions of maximum leaked field amplitudes in Fig. 4 for the simulation without He; these peaks are decreased in the run with He due to field ionization).

several Rayleigh lengths. In jet experiments, the existence of a neutral gas tail in front of the plasma channel is less likely in the coaxial ignitor-heater approach but could exist in axicon or transverse ignitor-heater experiments if the ionizing beam is too short. In such experiments, jet profiles show[25] a gas tail density of about 0.02 peak density and a length of several Rayleigh lengths.

Here, we have briefly explored the effect of a gas tail on the coupling of a laser pulse into a plasma channel. We simulated two cases. In both cases, the pulse propagates through a He gas tail of Z_r length before it reaches the plasma ramp. In the first case the tail gas density was set to $0.05n_0$, while in the second case it was increased by one order of magnitude to $0.5n_0$. After the gas density tail, the plasma density ramp was one Z_r long and He gas was placed on the sides of the plasma with the same profile as in the first simulation case in this section. In both simulations, the vacuum focus location and waist size were chosen according to their optimal values from the numerical solution of Eq. (4) with the boundary conditions (5). This model does not take into account the gas tail and considers the pulse propagates in vacuum before it reaches the plasma ramp. By choosing x_f and W_0 according to this model and propagating through a gas tail, we can explore the regime when the model is still approximately applicable and when the gas tail effect becomes important. Thus, in these simulations $x_f=211$ μm (approximately 71 μm from the top of the ramp) and $W_0=6.1$ μm.

The process of propagation of the pulse through part of the He gas tail, through the plasma ramp, and then into the channel is shown by the particle plot (including electrons, He^+ and He^{++} ions) in Fig. 6. This plot is done at a simulation time after the moving window has started and thus includes only part of the region of the He gas tail. In this region, $x \leqslant Z_r$ (141 μm), the He^{++} ions are in the domain in which the pulse is intense enough to doubly ionize He atoms. Then on the sides He^{++} domain there are two stripes of He^+ ions. At the location of these stripes, the intensity of the pulse is sufficient to ionize He atoms but not high enough to also further ionize He^+ ions. Outside of the domain of the stripes in the tail, the pulse does not have sufficient intensity to ionize He atoms. In this figure, the electrons are plotted

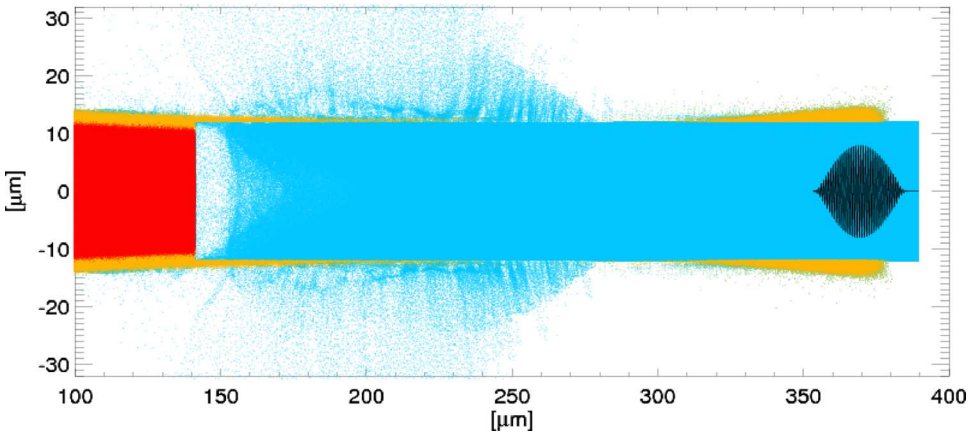

FIG. 6. (Color online) The configuration space locations of particles in a simulation with He gas tail and He on the sides of the plasma channel demonstrate the field ionization process and the behavior of electrons when the pulse moves through the ramp and couples to the channel. A scaled lineout of the E_z component of the electric field is shown at the longitudinal location of the pulse. The simulation is with a moving window that is currently turned on. The He gas tail ends at 141 μm (the pulse propagates through one Z_r length of He gas tail density). This is also the end of the domain of He^{++} ions (shown in red or dark gray in the black-and-white version of the figure) due to field ionization. The He^+ ions are shown in yellow (light gray) and electrons in light blue (medium gray). Note that the electrons are plotted first and mostly covered in the regions where He^+ and He^{++} ions are also present.

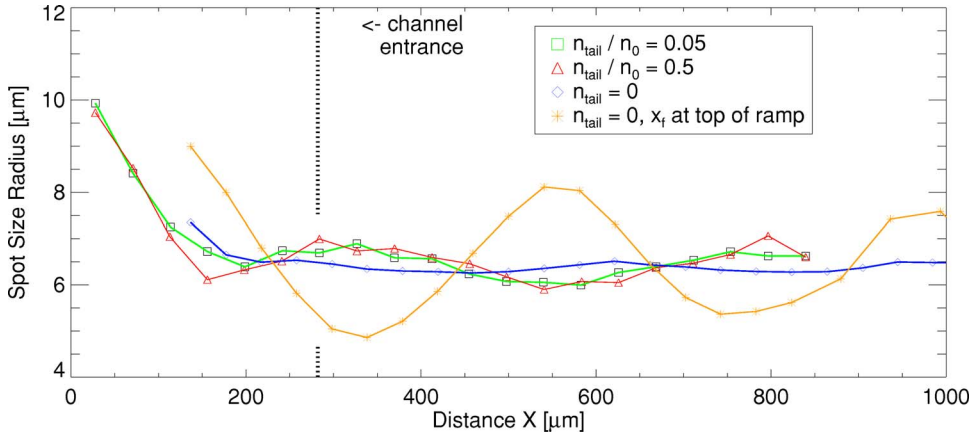

FIG. 7. (Color online) Propagation of a laser pulse through the He gas tail before it reaches the plasma channel ramp leads to suboptimal coupling to the channel. The spot size shows oscillations when the pulse propagates in the channel (data from two different He tail densities are shown with squares and triangles) relative to the best matched case (diamond symbols) when the pulse propagates in vacuum before it reaches the plasma channel ramp. However, the considered He tail densities affect the coupling much less than how the vacuum focus location and waist are chosen: the oscillations of the spot size when the vacuum focus is chosen at the top of the ramp and the waist is set to the value of the channel radius show oscillations with several times larger amplitude (star symbols).

first and are "screened" in the domains where He^+ and He^{++} ions are also present.

After the propagation through the He gas tail, the pulse enters the plasma ramp and the He gas on its sides. The region of the plasma ramp shows electrons blown outside of the ramp by the converging pulse. It is of interest that in the domains of the plasma ramp and channel shown in Fig. 6, the intensity of the pulse outside of the plasma is not sufficiently high to produce He^{++} ions. Moreover, close to the top of the ramp, the intensity of the pulse is well coupled to the plasma and there is practically no He gas ionization outside of the plasma.

In order to better evaluate the coupling of the pulse to the plasma channel in the simulations with a He gas tail, we calculated the spot size diagnostic from the beginning of the run to approximately $4Z_r$ propagation inside of the channel (about 850 μm total propagation distance). These results are shown in Fig. 7. In the same figure are also shown the results for the spot size behavior from the two runs with one Z_r-long ramp, without a He gas tail, and when the pulse vacuum focus and waist size are optimally chosen and at the top of the ramp. These are the two cases that are also shown in the top plot in Fig. 3. However, we have shifted the data for the runs without a gas tail along the x axis by a constant value when plotting them together with the spot sizes from the runs with gas tails in Fig. 7 in order to place the beginning of the plasma ramp (and the start of the channel) at the same location (it is indicated by vertical dotted line segments in Fig. 7).

The spot size behavior from the runs with He gas tails shows the appearance of spot size oscillations inside of the channel relative to the run with optimal parameters and no gas tail (diamond symbols). The amplitude of the oscillations is very similar for these runs despite a difference of one order of magnitude in the tail gas density between the two. These oscillations indicate that the efficiency of pulse coupling to the channel decreases when there is a He gas density tail. However, these oscillations are much smaller compared to the simulation with no He gas tail and when the vacuum focus location is placed at the top of the plasma ramp with vacuum waist size equal to the channel radius (the data with star symbols in Fig. 7). Thus, for these gas tail density parameters (tail length and He density), the tail affects the coupling, but from the spot size diagnostic this affect does not appear significant when the optimal vacuum focus location and waist size are chosen only taking into account the plasma density ramp via the model developed in Sec. II B. Extended parameter studies of configurations with gas tails, taking into account quantitatively such effects as blue shifting and steepening of the front of the pulse[26] due to the field ionization, will be considered in a separate study.

IV. SUMMARY AND CONCLUSIONS

We considered the problem of how to optimally couple a laser pulse to plasma channels in the presence of channel ramps with different lengths.

We derived an equation for the laser pulse spot size evolution in the plasma density, including the ramp. From numerical solutions of this equation, we determined the vacuum focus location and waist size that led to optimal coupling. These results show that for a laser pulse to couple optimally to a plasma channel with a ramp, the vacuum focus has to be chosen in the ramp and not at the channel entrance (the top of the ramp). The location of the vacuum focus in the ramp decreases by more than 40% from the position at the top of the ramp. This deviation increases when the ramp length increases. Moreover, for optimal coupling the waist size has to increase when increasing the length of the ramp. For the longest ramp studied here, $2Z_R$, this increase is close to 10% relative to the channel radius. These results are also confirmed by the data from 2D PIC simulations we did with the VORPAL code.

In this analysis, we considered that the ramp length and the channel radius are given. Then, we determined what the optimal values for the laser pulse vacuum focus location and

waist should be. But the equation we derived for the laser spot size evolution also allows us to solve the following inverse problem. For given laser pulse vacuum focus location and waist size, determine the plasma density ramp length and channel radius for the optimal coupling of the specified pulse. This could be valuable if one has a diagnostic for the plasma density (ramp and channel) evolution to determine the precise time when to launch the pulse for optimal coupling while keeping the pulse vacuum focus location and waist fixed.

We also developed two code diagnostics in VORPAL to investigate how laser pulses couple to plasma channels. The first diagnostic allows us to determine the laser spot size at any time during a PIC simulation. The results from this diagnostic show that when we launch a laser pulse with vacuum focus location at the top of the ramp and with waist size equal to the channel radius, large spot size oscillations are observed when the pulse propagates in the channel. The oscillations lead to an increase in pump depletion and leakage outside of the channel. The pulse does not couple efficiently to the channel. However, for the simulations with the optimal vacuum focus location (in the ramp) and waist size (larger than the channel radius), as obtained for different ramp lengths from the equation for the spot size evolution, the spot size oscillations are effectively suppressed. The simulations with these parameters show efficient pulse coupling and channel guiding.

Furthermore, we developed a space-time FFT power spectral diagnostic to study pump depletion and leakage using field data from PIC simulations. The results from this diagnostic also show that pump depletion is reduced when using the optimal laser pulse parameters relative to the simulations with the vacuum focus at the top of the channel ramp and the waist size set to the channel radius.

The pump depletion values obtained with the PSD diagnostic from the PIC simulations data are in good agreement with the predictions from a 1D theory.[15] The leakage outside of these channels is also reduced when we use the optimal pulse parameters relative to the simulations with the other pulse parameters. The leakage values are in reasonable agreement with a WKB theory[7] for the leakage out of the fundamental mode.

We also investigated the effect of field ionization of He on laser pulse coupling and guiding via PIC simulations. The He gas density was located outside of the plasma channel. We also explored briefly the effect that a He gas density tail in front of the plasma density ramp has on the coupling. The results show that field ionization of He and He^+ leads to increased pump depletion, particularly for the longest channel ramp, $2Z_R$, and the longest propagation distance in the channel. However, for the He densities we considered here and the optimal laser pulse coupling parameters (that we obtained from a theory for the spot size that does not include the effect of field ionization), the overall effect of field ionization did not modify the coupling significantly relative to the same simulation cases without the He gas. Extended parameter studies of the effect of the gas tail in front of the plasma will be a subject of a separate study.

Overall, the presented results show that appropriate focusing of laser pulses can be achieved for matched coupling into plasma channels with ramps relevant to LWFA experiments such that subsequent depletion, leakage, and spot size oscillations are minimized.

ACKNOWLEDGMENTS

This work is supported by the U.S. DOE Office of Science, Office of High Energy Physics under Grant Nos. DE-FG02-03ER83857, DE-FC02-01ER41178, DE-FG03-95ER40926, and DE-AC02-05CH11231, including use of NERSC facilities, and by Tech-X Corporation.

APPENDIX: DIAGNOSTICS FOR ENERGY LEAKAGE AND PUMP DEPLETION

1. Power spectral analysis diagnostic

Correct numerical diagnostics for the study of diverse processes in laser-plasma PIC simulations, such as pump depletion, leakage outside of a guiding plasma channel, and Raman instabilities, require a technique that can unambiguously determine how much electric and magnetic field energy is propagating forward or backward on the grid, within a range of frequencies and wave numbers near the central values for the laser pulse. We demonstrate here that simultaneous Fast Fourier Transforms (FFTs) in space and time can provide such diagnostics.

We apply FFTs in both space and time on components of the total electric field in the simulation box and then calculate the power spectral density (PSD) to determine existing wave signatures in the electric field. The power spectral density is defined here as the absolute value squared of the Fourier transform of a signal. We consider the Fourier transform of electric field components $E_\alpha(\mathbf{r},t)$, where $\alpha=x$, y, or z. The PSD at the point $(\mathbf{k},\omega)$ in this case is $|E_\alpha(\mathbf{k},\omega)|^2$, where

$$E_\alpha(\mathbf{k},\omega) = \mathrm{FFT}[E_\alpha(\mathbf{r},t)],$$

and FFT[…] denotes the fast Fourier transform.

The position of observed PSD peaks in $(\mathbf{k},\omega)$ space indicates the wave vector and frequency of waves. We calculate the integral (sum) of the power spectral density, i.e., the total power in the signal, to estimate pump depletion and leakage. Moreover, the location of the power spectrum peaks in $(\mathbf{k},\omega)$ space allows one to determine the direction of propagating wave signals in real space, given that the direction of time is fixed and known. In this way, we can determine the power spectral density of the laser pulse that is associated with waves traveling along the positive x direction. With this diagnostic, we can also concentrate on signals traveling backwards in space and forward in time.

We demonstrate this capability for 2D simulations in which we launch laser pulses in vacuum in different directions. These pulses are linearly polarized along the ignorable direction z and are loaded in the simulations using the functional form given by Eq. (1).

If we do an FFT in space along the longitudinal axis x, for a line though the middle of the pulse (the line $y=0$ in the simulations) and an FFT in time, then a pulse moving forward will show peaks in the PSD plot at (k_0,ω_0) and at

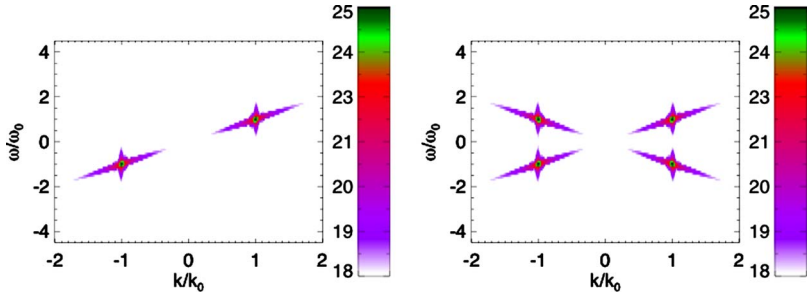

FIG. 8. (Color online) Images of the logarithm of the PSD for two simulation cases in vacuum. The left plot is for a laser pulse propagating along the (1, 0) direction. The peak in the first quadrant is at the pulse wave vector k_0 and frequency ω_0. The peak in the third quadrant is from an FFT that is a c.c. image of the PSD from the first quadrant. The right plot shows two counterpropagating pulses. This PSD diagnostic provides a direct capability to detect and distinguish forward- and backward-moving signals.

$(-k_0,-\omega_0)$ since the PSD of a real function is even. The appearance of these peaks in the calculated logarithm of the PSD (only the top seven orders of magnitude are shown) for a pulse moving to the right direction is shown in the left plot in Fig. 8.

The simulation box has $N_x=2400$ cells along x. The values of E_z are processed using FFT analysis in space using all 2400 points along the line $y=0$, although the pulse occupies approximately 600 cells at any instance of time. In contrast, the number of time data points used for the FFT along the time axis is 200. For all other results presented here, except the ones in Fig. 8, the number of time samples is 128. The time data are collected by dumping the electric field every N_t time steps, starting at a specific time in the simulation. Both the time samples and the cell spacing of the simulation grid are chosen to resolve the pulse wave vector and frequency. The cell size is chosen such that a pulse wavelength is sampled at least 16 times. The resolution along the time axis is chosen in the same way (usually sampling every time step). Since the FFT analysis uses only over 128 or 200 sample points in time, the resolution in frequency space is smaller than in wave-vector space. We use a Hanning window in the FFT calculations along both time and space. The Hanning transform over the time data is effective (to some extent) to suppress the Gibbs phenomenon since at the end points of the time sampled data, the signal in the transformed data generally has a nonzero value. However, even after applying the Hanning window over the time data, there are vertical bands of intensity at the main peak. The Gibbs oscillations can be further reduced by using more data points along the time axes and/or applying different window (kernel) functions in the FFT.[27,28] These further improvements will be considered elsewhere.

The plot on the right in Fig. 8 shows two counterpropagating laser pulses. One was launched from the left boundary of the simulation box, $x=0$, and the other from the right one, $x=N_x\Delta x$. For this case, in addition to the peaks from the forward propagating pulse, there are the peaks of the backward propagating pulse in the second quadrant at $(-k_0,\omega_0)$ and its symmetric image at $(k_0,-\omega_0)$. The application of this PSD diagnostic to estimate leakage from a plasma channel and pump depletion is discussed in Sec. II.

2. A 2D laser pulse rms width diagnostic

It is of importance to be able to determine robustly and accurately the local width of a laser pulse in laser-plasma PIC simulations. One such diagnostic is presented here for 2D and the pulse profile given by Eq. (1). For this case, the spot size for the laser pulse when it is at a location x can be approximated by the expression

$$W(x) \approx \sqrt{8/\pi} W_0 \langle E_z^2 \rangle / E_{z,\max}^2, \tag{A1}$$

where the average $\langle E_z^2 \rangle$ is calculated over the gridded field data of the PIC simulation at a fixed time from

$$\langle E_z^2 \rangle = \frac{1}{\lambda W_0} \int_{x-\lambda/2}^{x+\lambda/2} \int_{-\infty}^{+\infty} E_z^2(x',y,t)dx'dy \approx \frac{1}{2W_0} E_{z,\max}^2 \int_{-\infty}^{+\infty} \exp\left[-\frac{2(y-y_c)^2}{W^2(x)}\right] dy, \tag{A2}$$

where $E_{z,\max}$ is the maximum amplitude of the field at x. In the algorithm we implemented, the integral over y is represented by a sum over the data points along y that are in the simulation box.

Figure 9 illustrates our implementation of an algorithm to calculate Eq. (A1) for the case of a laser pulse propagating in vacuum. The focus of the pulse is placed in the center of the simulation box (100 μm) with a spot size of $W_0=6$ μm. Due to diffraction, the width of the pulse will vary as the pulse propagates according to Eq. (2) shown in the solid line. The pulse width obtained with the algorithm is shown in square dots. There is a good agreement between the analytical and computational (from the PIC data) results.

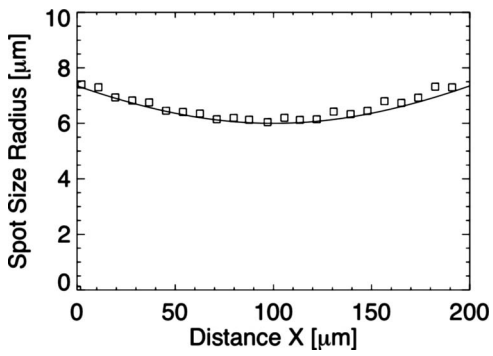

FIG. 9. Spot size width for a laser pulse propagating in vacuum with its focus placed at 100 μm. The solid line represents the analytical solution given by Eq. (2) and the square dots are the solution obtained by the algorithm.

[1] E. Esarey, P. Sprangle, J. Krall, and A. Ting, IEEE Trans. Plasma Sci. **PS-24**, 252 (1996).
[2] W. P. Leemans, B. Nagler, A. J. Gonsalves, C. Toth, K. Nakamura, C. G.

R. Geddes, E. Esarey, C. B. Schroeder, and S. M. Hooker, Nat. Phys. **2**, 696 (2006).
[3]C. G. R. Geddes, C. Toth, J. van Tilborg, E. Esarey, C. B. Schroeder, D. Bruhwiler, C. Nieter, J. Cary, and W. P. Leemans, Nature (London) **431**, 538 (2004).
[4]C. G. R. Geddes, C. Tóth, J. van Tilborg, E. Esarey, C. B. Schroeder, D. Bruhwiler, C. Nieter, J. Cary, and W. P. Leemans, Phys. Plasmas **12**, 056709 (2005).
[5]C. G. R. Geddes, C. Toth, J. van Tilborg, E. Esarey, C. B. Schroeder, J. Cary, and W. P. Leemans, Phys. Rev. Lett. **95**, 145002 (2005).
[6]C. Nieter and J. R. Cary, J. Comput. Phys. **196**, 448 (2004).
[7]P. Volfbeyn, E. Esarey, and W. P. Leemans, Phys. Plasmas **6**, 2269 (1999).
[8]P. Sprangle, J. R. Peñano, and B. Hafizi, Phys. Rev. E **66**, 046418 (2002).
[9]J. Moloney and A. Newell, *Nonlinear Optics*, 3rd ed. (Addison-Wesley, Redwood City, CA, 1992).
[10]D. L. Bruhwiler, R. E. Giacone, J. R. Cary, J. P. Verboncoeur, P. Mardahl, E. Esarey, W. P. Leemans, and B. A. Shadwick, Phys. Rev. ST Accel. Beams **4**, 101302 (2001).
[11]W. Leemans, C. W. Siders, E. Esarey, N. E. Andreev, G. Shvets, and W. B. Mori, IEEE Trans. Plasma Sci. **24**, 331 (1996).
[12]P. Sprangle, E. Esarey, J. Krall, and G. Joyce, Phys. Rev. Lett. **69**, 2200 (1992).
[13]W. H. Press, S. A. Teukolsky, W. T. Vetterling, and B. P. Flannery, *Numerical Recipes in C: The Art of Scientific Computing* (Cambridge University Press, New York, 1992), pp. 732–734.
[14]J. Wu, H. H. Cooley, T. M. Antonsen, and H. M. Milchberg, Phys. Plasmas **12**, 043105 (2005).
[15]D. Teychenné, G. Bonnaud, and J.-L. Bobin, Phys. Plasmas **1**, 1771 (1994).
[16]T. R. Clark and H. M. Milchberg, Phys. Rev. E **61**, 1954 (2000).
[17]J. P. Berenger, J. Comput. Phys. **114**, 185 (1994).
[18]S. D. Gedney, IEEE Trans. Antennas Propag. **44**, 1630 (1996).
[19]Tech-X Corporation, 5621 Arapahoe Avenue, Suite A, Boulder, CO 80303, *TxPhysics software library*, http://www.txcorp.com/technologies/TxPhysics/, URL http://www.txcorp.com/technologies/TxPhysics/.
[20]L. V. Keldysh, Sov. Phys. JETP **20**, 1307 (1965).
[21]A. M. Perelomov, V. S. Popov, and M. V. Terent'ev, Sov. Phys. JETP **23**, 924 (1966).
[22]A. I. Nikishov and V. I. Ritus, Sov. Phys. JETP **23**, 168 (1966).
[23]M. V. Ammosov, N. B. Delone, and V. P. Krainov, Sov. Phys. JETP **64**, 1191 (1986).
[24]N. B. Delone and V. P. Krainov, J. Opt. Soc. Am. B **8**, 1207 (1991).
[25]C. G. R. Geddes, Ph. D. thesis, University of California, Berkeley (2005).
[26]D. L. Bruhwiler, D. A. Dimitrov, J. R. Cary, E. Esarey, W. Leemans, and R. Giacone, Phys. Plasmas **10**, 2022 (2003).
[27]C. Lanczos, *Applied Analysis* (Dover, Mineola, NY, 1988), pp. 225–227.
[28]A. Weiße, G. Wellein, A. Alvermann, and H. Fehske, Rev. Mod. Phys. **78**, 275 (2006).